

# First tests of the coronagraphic device of MIRI/JWST

Céline Cavarroc<sup>a</sup> and Jérôme Amiaux<sup>a</sup> and Pierre Baudoz<sup>b</sup> and Anthony Boccaletti<sup>b</sup> and Patrice Bouchet<sup>a</sup> and Didier Dubreuil<sup>a</sup> and Pierre-Olivier Lagage<sup>a</sup> and Vincent Moreau<sup>a</sup> and Eric J. Pantin<sup>a</sup> and Jean-Michel Reess<sup>b</sup> and Samuel Ronayette<sup>a</sup> and Gillian S. Wright<sup>c</sup>

<sup>a</sup>CEA, IRFU/SAP, bât. 709, Orme des Merisiers, 91191 Gif-Sur-Yvette, France

<sup>b</sup>Observatoire de Paris-Meudon, 5 place Jules Janssen, 92195 Meudon, France

<sup>c</sup>Royal Observatory, Blackford Hill, Edinburgh, EH9 3HJ, Scotland, UK.

## ABSTRACT

One of the main objectives of the instrument MIRI, the Mid-InfraRed Instrument, of the JWST is the direct detection and characterization of extrasolar giant planets. For that purpose, a coronagraphic device including three Four-Quadrant Phase Masks and a Lyot coronagraph working in mid-infrared, has been developed. We present here the results of the first test campaign of the coronagraphic system in the mid-infrared in the facility developed at the CEA. The performances are compared to the expected ones from the coronagraphic simulations. The accuracy of the centering procedures is also evaluated to validate the choice of the on-board centering algorithm.

**Keywords:** JWST, MIRI, instrumentation, coronagraphy, optical testing

## 1. INTRODUCTION

MIRI, the Mid-InfraRed Instrument is one of the four instruments of the JWST planned to be launched in 2013 and placed at the second Lagrangian point. MIRI consists in an high resolution spectrograph and an imager, which includes also four coronagraphs and low resolution spectrograph.

Among the coronagraphs, three are monochromatic Four Quadrant Phase Masks<sup>1</sup> (hereafter FQPM) centered respectively at 10.65, 11.4 and 15.5 microns, which aim to detect and characterize Extrasolar Giant Planets<sup>2</sup>; the last one is a Lyot coronagraph centered at 23 microns and dedicated to the study of circumstellar disks. An optical device has been developed at CEA to validate the optical characteristics of the imager of MIRI (MIRIM). It associates a warm telescope and a model of the imager of MIRIM cooled down to 4 K inside a cryogenic enclosure.

This facility will be described in section 2. Qualification of the imager is presented elsewhere in the conference.<sup>3</sup> We present here results obtained on the FQPM centered at 10.65 microns; the performances of the coronagraph and its characteristics (rejection, inner working angle, sensitivity to pupilshear) are compared with the expected performances obtained from simulations in section 3. Finally we evaluate the accuracy of the algorithm proposed for centering the PSF on the coronagraph in section 4.

## 2. MID-INFRARED FACILITY

### 2.1. Specifications

#### 2.1.1. Optical characteristics

The telescope simulator reproduces the beam that the JWST will deliver to MIRI imager. The main optical characteristics of the JWST beam are listed below:

- FoV:  $72 \times 72 \text{mm}^2$

---

Further author information: (Send correspondence to C.C.)  
E-mail: celine.cavarroc@cea.fr

- Numerical aperture: F/20
- MIRIM entrance pupil diameter: 151.5mm
- Distance MIRIM entrance pupil to focal plane: -3021mm
- Uncertainty of pupil position (pupil shear): +/- 3.75%

The telescope simulator FoV is increased to  $80 \times 80 \text{mm}^2$  to account for positioning error of MIRIM in the cryostat.

### 2.1.2. Stability

The coronagraphy mode drives the specifications in terms of stability of the bench. An image of the point source must be stable within  $\pm 3 \mu\text{m}$  during 30 minutes. For this purpose, the whole system (telescope simulator, sources, cryostat) is set-up on 2 optical benches tightly linked together and mounted on anti-vibration pads. To avoid slow drift due to thermal variation, the room is equipped with air conditioning with temperature control.

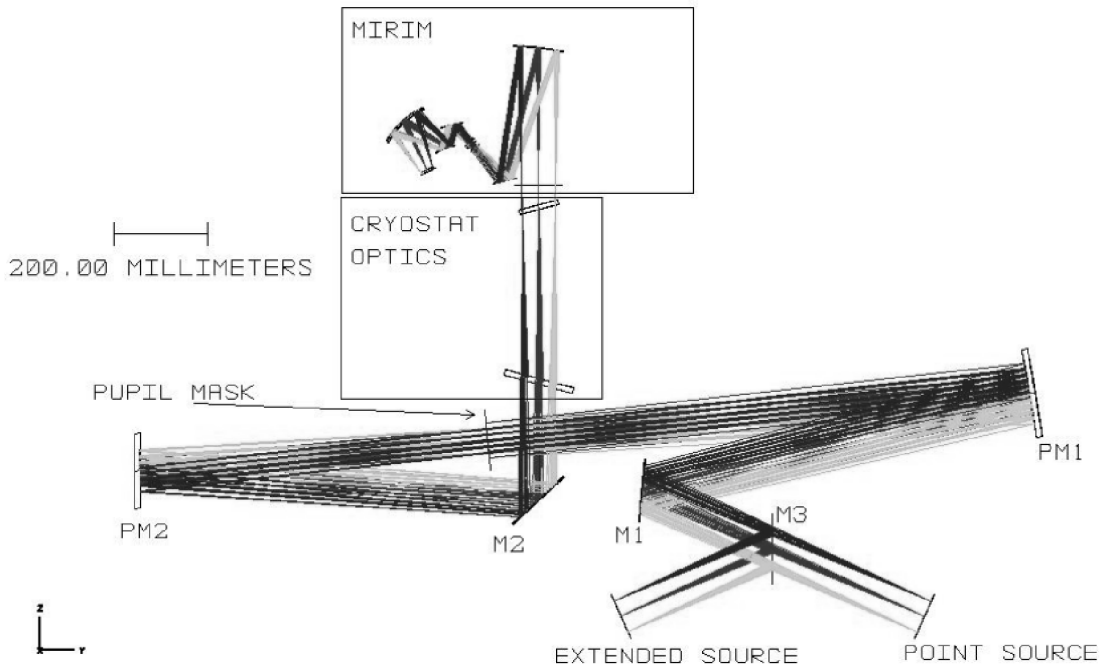
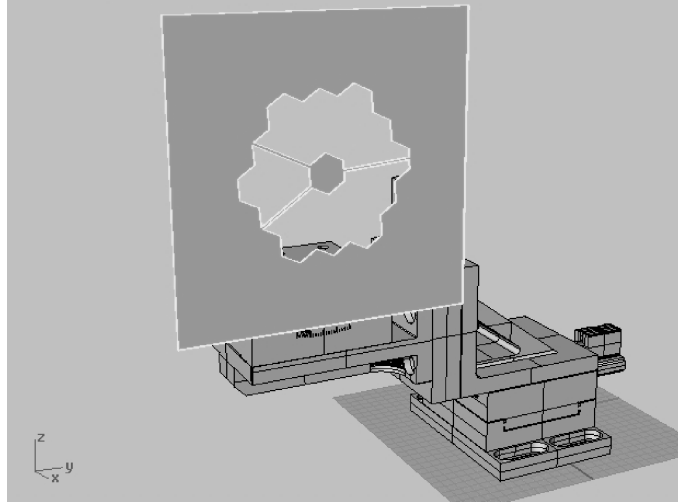


Figure 1. Optical layout of the test bench.

### 2.1.3. Sources

The telescope simulator allows illumination of MIRIM entrance focal plane with either an extended source or a point-like source. The extended source is a  $100 \times 100 \text{mm}^2$  flat black body with a surface temperature range of  $-5^\circ \text{C}$  to  $+100^\circ \text{C}$ . The uniformity is better than  $0.3^\circ \text{C}$ , with a temperature measurement accuracy of  $0.3^\circ \text{C}$ . The emissivity is 0.98. Again, the point source specifications are driven by the need for coronagraphy. The source is a LOT-ORIEL ceramic element with a temperature up to 2000K. The light is coupled to a  $30 \mu\text{m}$  pinhole. For tests less regarding in terms of source size and/or demanding more throughput, the pinhole can be changed for a larger one ( $50 \mu\text{m}$ ,  $80 \mu\text{m}$ ...up to 1mm). The source is mounted on a hexapod remotely controlled, with the following specifications:



**Figure 2.** 3D vue of the telescope simulator stop showing the JWST-like pupil used.

- Range of movement:  $80 \times 80 \text{mm}^2$  (focal plane) x 10mm (optical axis) minimum step:  $3 \mu\text{m}$ ,
- Positioning accuracy:  $\pm 1.2 \mu\text{m}$  within a  $30 \mu\text{m}$  range and  $\pm 10 \mu\text{m}$  within a 1.2mm range,
- Positioning repeatability: better than  $1.2 \mu\text{m}$  within a 1.2mm range.

## 2.2. Optical layout

An optical layout of the bench is shown in Fig. 2.1.2. This is a 1:1 magnification system, compound of 2 parabola and 2 flat mirrors to fold the beam. A third flat mirror allows switching between point source and extended source. The cryostat optics are composed by a Ge window and a Ge cold neutral density for limiting the background flux on the low capacity flight-like detector. The pupil mask is accurately positioned with respect to the PM2 mirror, in order to give the desired entrance pupil to MIRIM (see Fig. 2.2). It is mounted on motorized translation and rotation stages in order to do a fine adjustment and simulate pupil misalignment.

## 3. PERFORMANCES OF THE FQPM

To verify whether the results obtained on the test bench are compliant with expected performances on the sky, we will compare data with results obtained from simulations. Because of the use of a warm telescope, the thermal background is very high. So exposures are done in a 'chopping mode' where the chopping is realized by alternatively opening and closing of the entrance pinhole.

### 3.1. Centered PSF

The first point to study is the rejection of the coronagraph, i.e. the maximum of the coronagraphic image normalized by the maximum of the PSF.

Images obtained on the test bench are represented in Fig. 3 left: the upper image represents the coronagraphic PSF while the lower one corresponds to the residual light after the coronagraph. A central disk of residual light is clearly visible: it corresponds to the image of the support of the pinhole heated by the warm source. They correspond to an exposure time of 2 minutes and 50 secondes. Longer exposures have not be done because of a small drift in the facility which lead to a decentering of the source on the coronagraph.

We calculated the mean radial profiles of both images. The raw attenuation on the peak is 250. At larger angular separation, the contrast is limited by the background. They are represented on Fig. 3 right. We compare these results from those obtained from simulations (and plotted in Fig. 3 right by dashed lines).

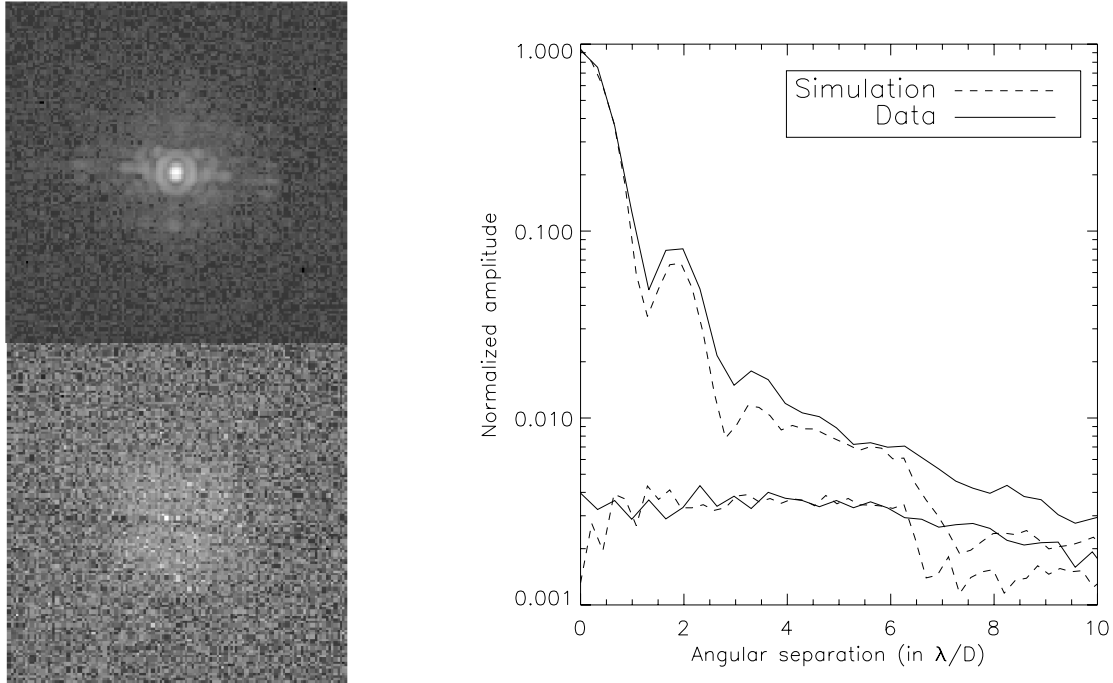


**Figure 3.** Comparison of performances of the coronagraph obtained of the bench to simulated ones. The left figure represents the image of the PSF (top image) and the coronagraphic image (bottom). In the right panel, the radial profiles of the results with a FQPM (lower curves) and without (upper curves) are plotted.



**Figure 4.** Optimized coronagraphic diaphragm. Its transmission is 53 %.

We have developed a numerical code which takes into account the different characteristics of the system:

- the JWST entrance pupil (see Fig. 2.2).
- the optimized Lyot diaphragm. It has been designed and optimized to reduce the diffraction in the second pupil plane and also to keep a high transmission. The diaphragm represented in Fig. 3.1, used in the optical bench but also included in the simulations, has a transmission of 53 %.
- the size of the pinhole: its diameter is 30 microns which reduces the performances of the coronagraph (at about 560 with the configuration of the warm telescope).

- the spectral bandwidth of the FQPM: the coronagraph will be operating with a spectral resolution of 20; the coronagraph being chromatic, this reduces again its nulling capacities.<sup>4</sup> This chromatism is simulated by adding monochromatic images between 10.38375 and 10.91625 microns.
- the sampling of the detector: it is about 3 pixels per  $\lambda/D$  at 10.65 microns.
- we add the noise estimated from the measures made on the test bench.

Agreement between measures and data is good which confirms that the FQPM behaves as expected. The main differences come from the estimation of the noise.

### 3.2. Attenuation as a function of the angular separation

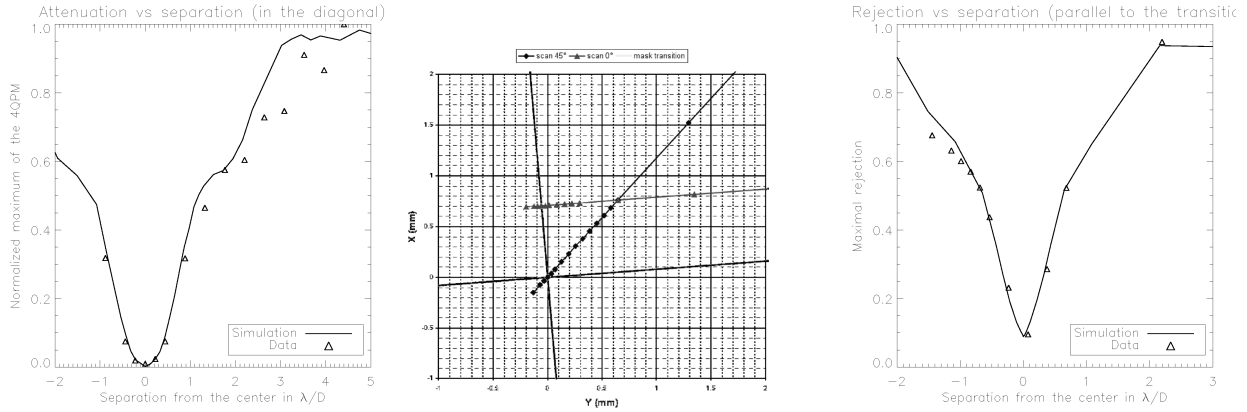


**Figure 5.** Attenuation due to the coronagraph with respect to the angular separation.

The left figure represents the attenuation of the coronagraph crossing the center of the coronagraph in diagonal, the middle one is a scheme of the different positions of the PSF and the right one represents the attenuation of the coronagraph crossing a transition parallelly to the other one.

One of the great interest of the FQPM is its small inner working angle (hereafter IWA) compared to the classical Lyot coronagraph which IWA needs to be at least  $3 \lambda/D$  to be efficient. This small inner working angle is all the more interesting that MIRI will work in mid-infrared where the angular resolution is low.

So we will estimate this IWA and, for that purpose, we will study the attenuation as a function of the angular distance from the center of the coronagraph.

To do it we have moved the point source on different points, represented in Fig. 5 (center) to study the IWA crossing the center of the FQPM in diagonal (see Fig. 5 (left)). We define here the IWA as the smaller angle for which the transmission is higher than 50 %. We see that results (triangles) are in accordance with the simulated ones (plain line). In this simulation we do not consider the limitation due to the background noise because, except for central points, the signal-to-noise ratio is sufficiently high and the noise is not limitative. In this case, the IWA is  $1.2 \lambda/D$  but it is enlarged because of the size of the pinhole. Simulations are again compliant with the results obtained in the testbench.

We also study the size of the 'dead zones', the area where the transition absorbs the flux of the planet and will reduce its detectability. This effect is represented in Fig. 5 (right). In the transition, the maximum attenuation is 11, conformely to the simulations. Here the IWA is  $0.63 \lambda/D$ .

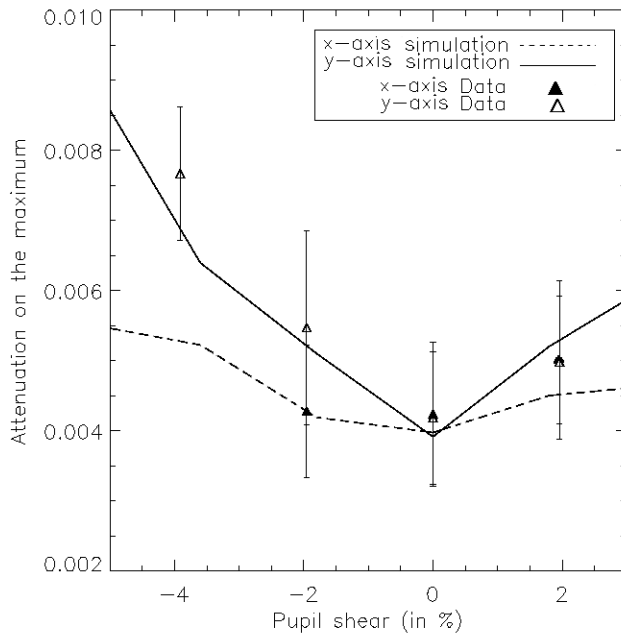


**Figure 6.** Attenuation due to the coronagraph with respect to the pupil shear in the two directions.

### 3.3. Impact of the pupil shear

Another aspect we have to study is the pupil shear. In MIRI, the pupil shear is specified to be lesser than 3.8 % of the pupil diameter. Simulations have proved that, on MIRI, the rejection maximum is expected to be degraded by a factor 3.5 from 0 to 4.5 % of pupil shear. This degradation increases faster at larger angular separation but this cannot be evaluated on the test bench because of the high background which limits the contrast.

We study now the impact of this pupil shear on the performances of the coronagraph. We only study the impact on the maximum rejection. The main difficulty comes from the signal-to-noise ratio which is very poor in this case. Results are presented in Fig. 6. Error bars correspond to the standard deviation of the noise at  $1\sigma$ . The asymmetry on the attenuation on the x-axis compared to the one on the y-axis is due to the asymmetry of the pupil and of the coronagraphic diaphragm.

## 4. CENTERING ALGORITHM

One of the main constraint to reach accurate performances on the FQPM is the centering. We have proved<sup>5</sup> that a precision of 7 mas was needed in the positioning of the coronagraph. Among this error budget, 3 mas are allocated to the algorithm. The chosen algorithm is the floating window center of gravity. It consists in an iterative center of gravity which uses portions of pixels to reduce the bias of the classical center of gravity. Another difficulty lies on the distortion and on the attenuation of the PSF when centered on the coronagraph. A means to reduce this effect is to use the properties of chromaticity of the coronagraph and to use it in a filter in which the coronagraph is not very efficient and less attenuates the flux of the source.

A neutral density has been developed for MIRI and its effect has been studied by.<sup>5</sup> In the testbed the only available interesting filter is the filter centered at 5.6 microns. But it must be noted that at this wavelength the image is not Nyquist sampled (Nyquist sampling is reached beyond 7.7 microns). The figure 7 left represents the shape of the PSF centered (top) and decentered (bottom) with respect to the PSF: the PSF is elongated because

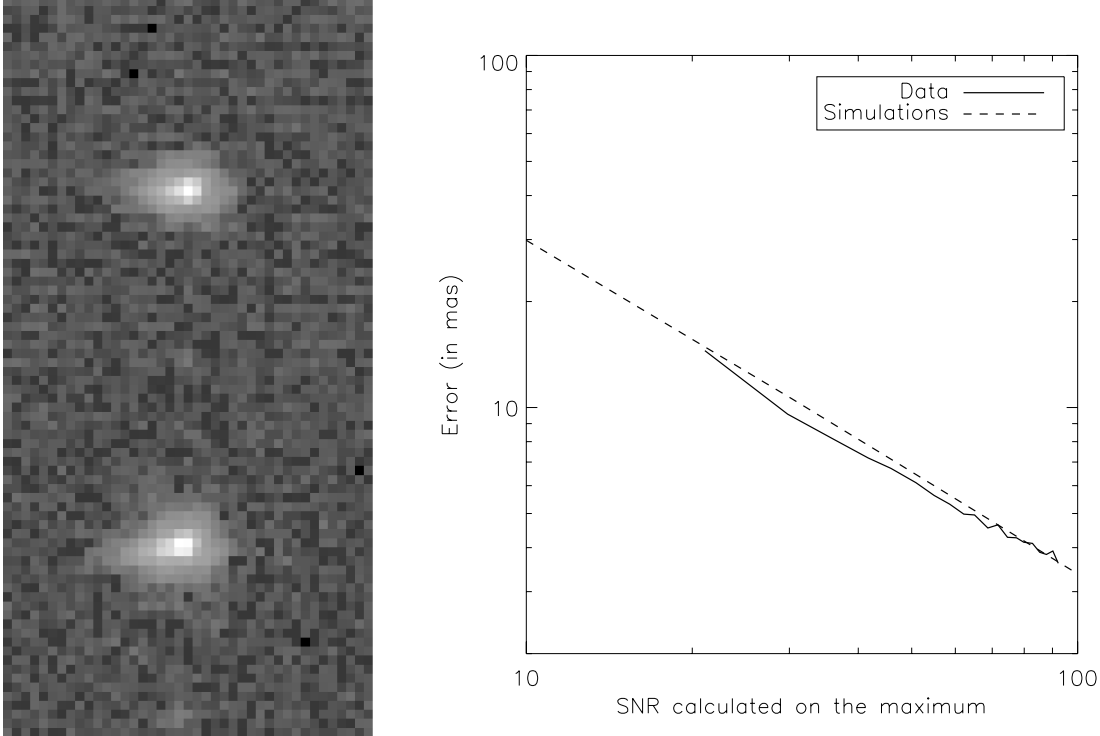


**Figure 7.** Peakup results.

The left panel represents the shape of the PSF at 5.6 microns on (top) and outside the coronagraphic mask (bottom). The right one represents the precision of the algorithm (the floating window center of gravity) with respect to the signal-to-noise ratio calculated on the maximum of the PSF.

of a ghost located at 3 pixels on the left of the PSF but in both cases (source centered on the coronagraph or not) the image has the same shape.

We compare results obtained on the testbench with those obtained in simulations. They include photon noise, read-out noise and background photon noise. We also consider the spatial and spectral resolution of the PSF using the filter centered at 5.6 microns. We can see in Fig. 7 right that simulations are compliant with data obtained on the bench. The plot represents the evolution of the estimation error of the algorithm as a function of the signal-to-noise ratio. It is estimated by calculating the standard deviation between the different estimations of the center of gravity. Oscillations on the curve obtained from data beyond the SNR of 60 is oscillating because the standard deviation is not calculated with enough points. The required 3 mas RMS would be reached with a SNR of about 140 which represents an exposure time of 0.5 s in MIRI with the 5.6  $\mu\text{m}$  filter.

## 5. CONCLUSION

To validate the coronagraphic system of the instrument MIRI a mid-infrared testbench, which associates a warm telescope simulator and a cryogenic instrument, has been developed at CEA. In this device, the main limitation comes from the high thermal background. We have studied here the FQPM centered at 10.65 microns with the JWST entrance pupil and the coronagraphic optimized diaphragm. Performances are compliant with that we were expecting. We have tested the raw performances of the FQPM and we have reached a maximum attenuation of about 250 limited by the background and the emission of the support of the pinhole. We also emphasize the interest of the FQPM compared to the Lyot coronagraph in particular in terms of IWA which is only  $1.2 \lambda/D$ . We have also studied the sensitivity to the pupshear. Finally, we have verified that the accuracy of the centering algorithm corresponds to the expected one.

Several other tests are foreseen to completely qualify MIRI. The entire instrument will be studied at the Rutherford Appleton Laboratory with a cryogenic telescope; there, photometry will be accurately estimated. Another campaign to test the flight model will take place at the CEA next december. It will allow us to get some missing informations because of the lack of signal-to-noise (defocus for instance).

## REFERENCES

1. D. Rouan, P. Riaud, A. Boccaletti, Y. Clénet, and A. Labeyrie, “The Four-Quadrant Phase-Mask Coronagraph. I. Principle,” *PASP* **112**, pp. 1479–1486, Nov. 2000.
2. A. Boccaletti, P. Baudoz, J. Baudrand, J. M. Reess, and D. Rouan, “Imaging exoplanets with the coronagraph of JWST/MIRI,” *Advances in Space Research* **36**, pp. 1099–1106, 2005.
3. J. Amiaux, F. Alouadi, J. L. Auguères, P. Bouchet, M. Bouzat, C. Cavarroc, C. Cloué, P. De Antoni, D. Desforge, A. Donati, D. Dubreuil, D. Eppelle, F. Gougnaud, P.-O. Hervieu, B. and Lagage, D. Leboeuf, I. Le Mer, P. Mattei, F. Meigner, V. Moreau, E. J. Pantin, P. Perrin, S. Ronayette, G. Tauzin, S. Poupard, D. Wright, A. C. H. Glasse, G. S. Wright, E. Mazy, J.-Y. D. Plessier, E. Renotte, T. Ray, A. Abergel, P. Guillard, Y.-Y. Longval, M. Ressler, J.-M. Reess, R. Hofferbert, O. Krause, K. Justtanont, and G. Olofsson, “Development approach and first infrared test results of JWST/mid-infrared imager optical bench,” *SPIE*, 2008.
4. P. Riaud, *Coronographie à masque de phase : applications aux télescopes et interféromètres au sol et dans l’espace*. PhD thesis, Université de Paris- Pierre et Marie Curie, 2003.
5. C. Cavarroc, A. Boccaletti, P. Baudoz, J. Amiaux, and M. Regan, “Target acquisition for MIRI coronagraphs,” *PASP submitted*.